PHYSICAL REVIEW A **89**, 023420 (2014)

Disclosing intrinsic molecular dynamics on the 1-fs scale through extreme-ultraviolet pump-probe measurements

P. A. Carpeggiani,[1,2] P. Tzallas,[1,*] A. Palacios,[3] D. Gray,[1] F. Martín,[3,4] and D. Charalambidis[1,2]

[1]*Foundation for Research and Technology–Hellas, Institute of Electronic Structure and Lasers, P.O. Box 1527, GR-711 10 Heraklion, Crete, Greece*

[2]*Department of Physics, University of Crete, P.O. Box 2208, GR71003 Heraklion, Crete, Greece*

[3]*Departamento de Química, Módulo 13, Universidad Autónoma de Madrid, 28049 Madrid, Spain*

[4]*Instituto Madrileño de Estudios Avanzados en Nanociencia (IMDEA-Nanociencia), Cantoblanco, 28049 Madrid, Spain*

(Received 17 December 2013; published 18 February 2014)

Through frequency up-conversion of polarization-shaped, femtosecond laser pulses nonlinearly interacting with xenon atoms, energetic, broadband, coherent, XUV continuum radiation is generated. By exploiting the thus-formed short-duration XUV pulses, all the optically allowed excited states of H_2 are coherently populated. Nuclear and electronic 1-fs-scale dynamics are subsequently investigated by means of XUV-pump–XUV-probe measurements, which are compared to the results of *ab initio* calculations. The revealed dynamics reflects the intrinsic molecular behavior, as the XUV probe pulse hardly distorts the molecular potential.

DOI: 10.1103/PhysRevA.89.023420 PACS number(s): 32.80.Rm, 42.65.Re, 42.65.Ky

I. INTRODUCTION

Coherent light pulses of few to hundreds of femtoseconds (fs) duration have prolifically served the field of ultrafast phenomena. While femtosecond pulses address mainly dynamics of nuclear motion in molecules or lattice in the gas, liquid, or condensed matter phase, the advent of attosecond (asec) pulses has in recent years provided direct experimental access to ultrafast electron dynamics. However, there are processes involving nuclear motion in molecules and in particular, coupled electronic and nuclear motion that occur in the few femtoseconds or even subfemtosecond time scale. Electronic excitations in molecules are commonly in the VUV–XUV spectral region. Until recently, most of the XUV sources were lacking either sufficient pulse energy [high harmonic generation (HHG) sources] or ultrashort pulse duration [free electron lasers (FEL)], thus preventing access to XUV-pump–XUV-probe measurements in the 1-fs or asec temporal scale. Experimental efforts in this time scale have been restricted to XUV-IR pump-probe schemes [1–7] or *in situ* electron-ion collision methods [8]. Systematic developments in high-pulse-energy HHG [9–13] and XUV supercontinua [14–19] paved the way to time-delay spectroscopic studies [20] and XUV-pump–XUV-probe experiments [21,22] that have lately demonstrated their first proof-of-principle application in the measurement of induced, ultrafast evolving atomic coherences in an atomic continuum [20,22]. Such measurements are free of interventions from unwanted channels, opened through quasiresonant multi-IR–photon transitions. The present work, motivated by a recent theoretical study [23], demonstrates a 1-fs-scale, XUV-pump–XUV-probe study of ultrafast dynamics in H_2. It further aims at illustrating a fundamental difference between atomic and molecular dynamics. In molecules the nuclear motion modulates the signal of the beating between coherently excited electronic states as the pumped target evolves field free, because the nuclear wave packet associated with each electronic state is moving and spreading, therefore modifying the relative contribution of the electronic states involved. In this work, a broadband XUV pulse is used to coherently excite all the optically allowed excited states of H_2. Nuclear and electronic dynamics are subsequently analyzed. These reflect the intrinsic molecular behavior, as the XUV probe pulse hardly distorts the molecular potential.

II. THE XUV-PUMP–XUV-PROBE SCHEME

The scheme under investigation is shown in Fig. 1(a). The inset shows the spectrum of the continuum radiation used. Absorption of one photon coherently excites all optically allowed electronic states of H_2, in each of which a superposition of those vibrational levels that are within the Franck-Condon region is populated. A fraction of the bandwidth also ionizes the molecule, leaving it in the bound part of the H_2^+ ionic ground state. The dynamics of the excited electronic and vibrational wave packets are probed through absorption of a photon from the second temporally delayed XUV pulse. Absorption of the second photon brings the molecule above its ionization limit at excess energies that allow fragmentation of the ion. Upon evolution of the molecular vibration, the molecule stretches to internuclear distances from which the $^2\Sigma_g^+(2p\sigma_u)$ state is accessible through the absorption of the second photon. Fragmentation through this repulsive state produces protons with nonzero kinetic energies that depend on the internuclear distance at the moment of the absorption of the second photon. Consequently, the delay is a parameter that can switch this channel on and off and control the kinetic energy of the produced protons. Although there is some probability that two photons are also absorbed either solely from the first or the second pulse, for the pulses used here, the $^2\Sigma_g^+(2p\sigma_u)$ state is dominantly populated through one-photon absorption from the first pulse followed by one-photon absorption from the second pulse, i.e., only through the pump-probe sequence.

III. THE EXPERIMENT

The experimental setup used has been described in previous works [14,16,20,21,24–26]. A 10-Hz repetition rate

*ptzallas@iesl.forth.gr

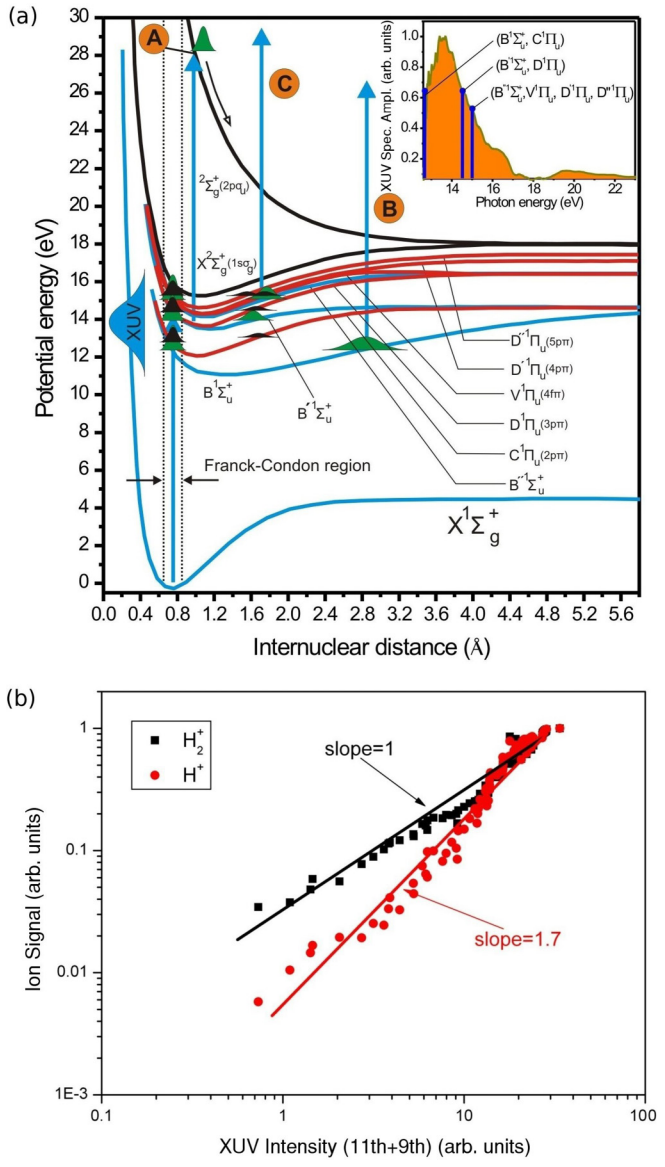

FIG. 1. (Color online) (a) The two-photon XUV resonant ionization-fragmentation scheme of H_2. The inset shows the XUV spectrum [green line (orange-filled area)] used in the experiment. (b) Ion yield dependence of H_2^+ and H^+ on the XUV intensity. The measured slopes of 1 and 1.7 are indicative of a linear and a two-photon process underlying the production of H_2^+ and H^+, respectively.

Ti:sapphire laser system delivering pulses of ≤170 mJ/pulse energy, 33-fs duration, and a carrier wavelength at 800 nm was used for the XUV generation. A laser beam of ≈2.8 cm outer diameter and energy of ≈100 mJ/pulse was passed through an interferometric polarization gating (IPG) device [14,16]. The ellipticity-modulated laser field, focused by a 3-m focal length lens, interacted with the atoms of a xenon gas jet, generating a coherent XUV continuum. The laser focus was placed before the jet in order to select mainly the short electron trajectory. The XUV was separated from the IR radiation through reflection on a Si plate placed at the Brewster angle for 800 nm. The XUV spectral region used in the experiment was selected by a 150-nm-thick indium filter that also filters out the residual IR radiation. The filter quality, in terms of IR transmission, was checked by means of an IR-XUV-beam profiler placed behind the filter foil, and the energy of the XUV radiation was measured using a calibrated XUV photodiode. The focus of the XUV beam in the detection area was characterized by means of an ion microscope detector [27]. The emitted XUV spectrum was recorded by measuring the energy-resolved photoelectron spectrum of the single-photon ionization of Xe. In the interaction area, the XUV pulse impinges at normal incidence a spherical split mirror of 10-cm radius of curvature. The mirror focuses the XUV beam into a pulsed H_2 jet, synchronized with the arrival of the XUV pulses. The XUV waist diameter is measured to be 2 ± 1 μm, and the estimated XUV intensity at the focus lies between 10^{13} and 10^{14} W/cm^2. Charged interaction products, i.e., H_2^+ ions and H^+ fragments, are detected through a time-of-flight mass spectrometer as a function of the delay introduced by the split mirror translating one of its two parts using a piezoelectric linear translator. The temporal resolution of the device is 150 asec. The overall temporal resolution is determined by the XUV pulse duration (>600 asec Fourier-transform-limited value), which is not measured because of the unstabilized carrier-envelope phase of the driving field, which causes an alternating XUV wave form from single-pulse to double-pulse structure [21,22,28]. While specific proton kinetic energies cannot be resolved in the mass spectrum, protons with nearly zero kinetic energy can be effectively distinguished from those with nonzero kinetic energy in the mass peak structure. Nearly zero kinetic energy fragments contribute mainly to the center of the ion-mass peak, while nonzero kinetic energy fragments are present mainly at the tails of the peak.

IV. RESULTS AND DISCUSSION

Observable two-XUV-photon absorption is verified through intensity dependence measurements of the ion yields shown Fig. 1(b). In log-log scale, the slope of H_2^+ yield is 1, as expected for a linear process, while the slope of the proton yield is close to 2 (1.7), indicative of a two-photon process. The XUV bandwidth used is rather advantageous, as it is broad enough to efficiently launch a nuclear wave packet that favors sequential two-photon absorption to the $^2\Sigma_g^+(2p\sigma_u)$ continuum and decreases the relative importance of one- and two-photon absorption to the $X^2\Sigma_g^+(1s\,\sigma_g)$ continuum [29].

For the numerical calculations we employ a method widely described in [23] and references therein. In brief, we solve the time-dependent Schrödinger equation

$$i\frac{\partial}{\partial t}\Phi(\mathbf{r},R,t) = [H(\mathbf{r},R) + V(\mathbf{r},R,t)]\Phi(\mathbf{r},R,t),$$

where r stands for the electronic coordinates, H is the Hamiltonian of the isolated molecule, and V is the laser-molecule interaction. The time-dependent function is written in the basis of the vibronic eigenstates of H_2. The initial wave function, $\Phi(\mathbf{r},R,t=0)$, is that of the ground state of the neutral, $X^1\Sigma_g^+$. The time-dependent potential term V is written in the dipole approximation as the product of the dipole operator and the potential vector $\boldsymbol{\mu}\cdot\mathbf{A}(t)$. The field is defined with two identical pulses with a given delay τ. The vector

potential can be then written as

$$\mathbf{A}(t) = A_0[F(t) + F(t-\tau)]\mathbf{e}_z,$$

where the direction of the field $\mathbf{e}_z$ is chosen parallel to the molecular axis, which implies that only transitions ${}^1\Sigma_g^+ \rightarrow {}^1\Sigma_u^+ \rightarrow {}^1\Sigma_g^+$ are included in the calculation. We use a sin-squared pulse with the form

$$F(t') = \begin{cases} \sin^2\left(\frac{\pi t'}{T}\right)\cos(\omega t' + \varphi) & t' \in [0,T] \\ 0, & \text{elsewhere} \end{cases}.$$

We define the pulses with a length $T = 2$ fs, which approximately corresponds to an experimental FWHM duration of 800 asec and a central photon energy $\hbar\omega = 14$ eV. The large energy bandwidth (~3 eV) of such a short pulse will populate bands of vibrational states associated to several electronic excited states. For simplicity, phase φ is equal to zero.

Figure 2 depicts a measured temporal trace of the total proton yield as a function of the delay between the two XUV pulses, while Fig. 3 shows the yield of protons with nonzero kinetic energy. It should be noted that protons with near-zero initial velocity component along the time-of-flight (TOF) axis (i.e., those contributing to the center of the mass peak, which we refer to as zero-kinetic-energy protons) are not only those with zero initial kinetic energy (irrespective of the molecule's orientation), but also most protons ejected perpendicularly with respect to the TOF. Thus protons with nonzero kinetic energy are mainly those ejected from molecules oriented perpendicularly to the polarization direction.

A nontypical but common feature in both figures is the local minimum observed at zero delay, at which the optical interference is expected to lead to a maximum yield in a

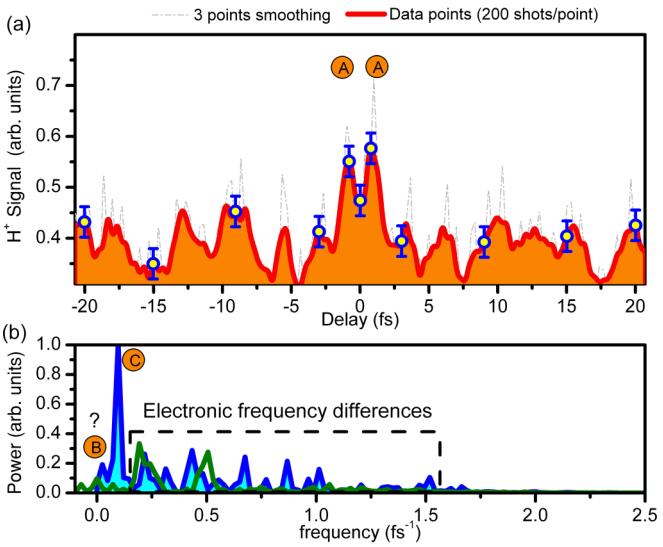

FIG. 2. (Color online) (a) Measured temporal trace of the total proton yield and (b) Fourier transform spectra of Figs. 2(a) and 3 traces. In (a), the observed minimum at zero delay and the succeeding buildup of the proton yield during the first 1 fs of delay is attributed to the dynamics of the opening of the dissociation channel through the ${}^2\Sigma_g^+(2p\sigma_u)$ repulsive potential. A, B, and C as in Fig. 1. The Fourier transform spectra of Figs. 2(a) and 3 are shown by the blue (blue-filled area) and green curve, respectively.

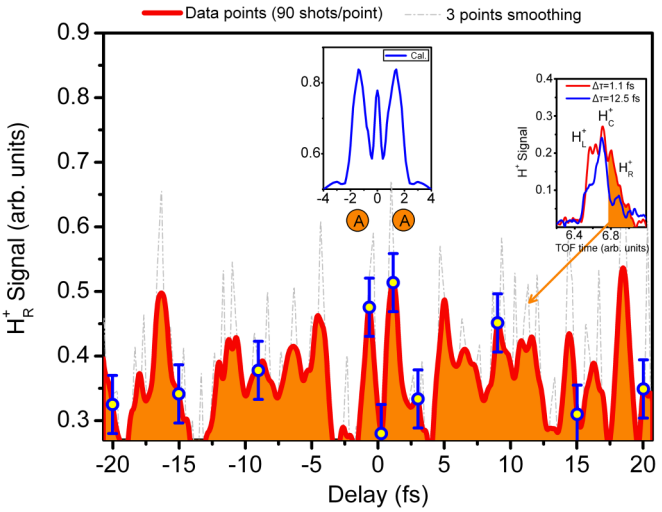

FIG. 3. (Color online) Measured temporal trace of the yield of nonzero kinetic energy photons [gray dashed and red line (orange-filled area)]. The minimum at zero delay and the yield buildup within the first femtosecond is also observable here as in Fig. 2. The blue curve (center inset) represents theoretical calculations, in which only intermediate states of Σ symmetries have been considered. The inset on the right depicts two ion-mass peaks measured at 1.1 fs (red line) and 12.5 fs (blue line) delays. At the $H_R{}^+$ edge (orange filled area) is the contribution of non-zero kinetic energy protons released towards the repeller of the TOF spectrometer. At the $H_L{}^+$ edge is the contribution of non-zero kinetic energy protons released towards the entrance of the TOF spectrometer. At the central $H_C{}^+$ part of the peak is the contribution of protons produced with zero velocity components parallel to the TOF axis.The amplitude of the H^+ signal around the zero delay values in this trace is smaller compared to the signal in the trace of Fig. 2(a) due to the absence of a "background" signal, which results from the measurement of zero-kinetic-energy H^+ ions. The background signal is the 2-IVAC trace averaged for alternating single- and double-XUV pulses resulting from a nonstabilized CEP IR pulse.

second-order process. This minimum and the subsequent buildup of the proton yield during the first femtosecond are attributed to the following dynamics. At zero delay, the dissociation channel through the ${}^2\Sigma_g^+(2p\sigma_u)$ state is practically closed, while after ≈1 fs the excited molecule stretches such that absorption of the second photon from the intermediate state reaches the repulsive state ${}^2\Sigma_g^+(2p\sigma_u)$, leading to an enhancement of the proton yield. At larger delays the yield decreases due to the wave-packet delocalization. Beyond their common feature around the zero delay, Figs. 2(a) and 3 preserve a significant difference, which is the signal ratio between near-zero and longer delay times. In the trace of Fig. 2(a), the signal around zero delay is significantly stronger compared to that at longer delay times, a feature that is missing in the trace of Fig. 3. The signal in Fig. 2(a) results from the convolution of the pump-probe channel and the "direct" two-photon absorption channel. Thus the increased yield in Fig. 2(a) results from the convolution of the second-order intensity volume autocorrelation (IVAC) maximum [24], with the dynamic effect of the dissociation channel opening. The nonzero kinetic energy protons of Fig. 3 start being produced at nonzero delays, for which only the tails of the two pulses

are overlapping, and thus the "direct" two-photon absorption is significantly reduced. The blue curve in the central inset of Fig. 3 has been obtained from the theoretical calculations. In these calculations, the contribution from protons with kinetic energy release of <0.4 eV has been removed. The narrow spike at zero delay is the second-order autocorrelation (AC) of the pulse used in the calculations. For a 720-asec-long pulse, its FWHM is 1.02 fs. As its width is smaller than the separation of the two side maxima, it is observable between them. The theoretical data in the spike region have been corrected for the reduced peak to background ratio of the second-order volume AC, contributing to the measured trace, as compared to that of a conventional second-order AC produced by the calculation. This spike is not observable in the measured trace for the following reasons. Since the laser system has an unstabilized carrier-envelope phase (CEP), the emitted XUV spectra fluctuate shot to shot between continuum and quasidiscrete spectra with variable harmonic peak positions [21]. Equivalently, the emitted XUV wave forms fluctuate from shot to shot between isolated pulses and double-peaked distributions with fluctuating relative peak heights. The corresponding shot-to-shot energy shift of the spectral distributions amounts to up to ± 1.5 eV. Moreover, the harmonic generation process produces non-Fourier-transform-limited pulses. For these reasons the measured second-order AC peak is broader than the distance between the two side maxima and thus appears as enhanced background.

The traces of Figs. 2(a) and 3 at longer delays depict similar features of multifrequency beating. Unlike in many existing studies, this beating is the result of combined electronic and vibrational wave-packet dynamics. The concurrent coherent excitation of electronic and vibrational states in principle allows the simultaneous investigation of electronic and nuclear motion. The vibrational frequencies and energy differences of different states are shown in the theoretical curves of Fig. 4. The Fourier transform (FT) of the traces in Figs. 2(a) and 3 is shown in the blue (blue-filled area) and green curves, respectively, in Fig. 2(b). In the FT of Fig. 2(a), the pronounced peak at 0.09 fs^{-1} corresponds to half the vibrational period of the $C\,^1\Pi_u$, $B'\,^1\Sigma_u^+$, $D\,^1\Pi_u$(unresolved) states at the excitation energy interval of the experiment [30], the $C\,^1\Pi_u$being the main contributor. This is the only frequency peak that can be safely assigned in the present work. The small peak at 0.04 fs^{-1} is compatible with half the vibrational period of the $B\,^1\Sigma_u^+$ state, but due to the maximum delay of the measured trace (± 22 fs), such a measurement is marginal. In the FT of Fig. 3 [green curve in Fig. 2(b)], the pronounced peak C disappears. This is compatible with the fact that states of Π_u symmetry (in particular, the $C\,^1\Pi_u$ state) do not contribute to the nonzero kinetic energy proton yield. (The $\Sigma_g \rightarrow \Pi_u$ transition is forbidden for molecules parallel to the polarization direction.) The rest of the peak structure in the FT spectra could be attributed to beating frequencies between electronic states.

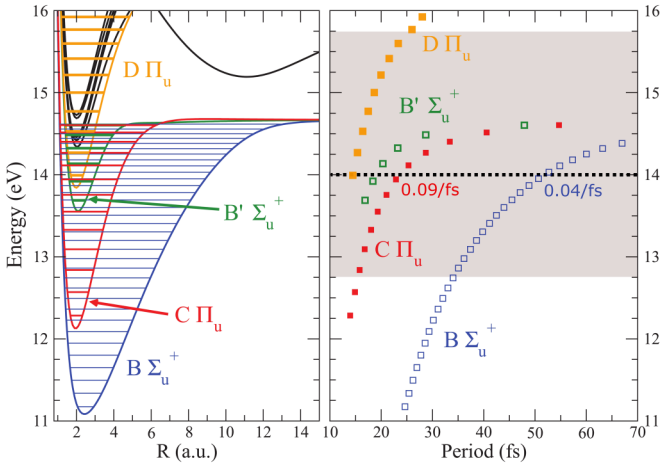

FIG. 4. (Color online) Potential curves and vibrational levels of the first four excited electronic states of H_2 (left). Estimated vibrational periods of the four states as a function of the excitation energy (right). The shaded area is the spectral area covered by the experimental spectral width of the XUV radiation.

The signal level and spectral resolution of the experiment do not allow an unambiguous assignment of these peaks.

V. CONCLUSIONS

In summary, utilizing an intense coherent XUV supercontinuum radiation, simultaneous electronic and nuclear dynamics in molecular hydrogen, evolving at the 1-fs temporal scale, have been studied by means of an XUV-pump–XUV-probe experiment. The present work paves the way to studies of dynamics beyond the Born-Oppenheimer approximation, addressing the dependence of the electronic dynamics on the variation of the internuclear distance during the vibrational motion. This will be achieved at increased temporal resolution through reduced pulse duration, while the recording of long temporal traces will substantially improve resolution in the frequency domain.

ACKNOWLEDGMENTS

This work is supported in part by the European Commission programs ATTOFEL, CRISP, Laserlab Europe, the European COST Actions MPI1203-SKO and CM1204 XLIC, and the Greek funding program NSRF. A.P. and F.M. acknowledge allocation of computer time by CCC-UAM and BSC Mare Nostrum, and financial support from the Advanced Grant of the European Research Council XCHEM (No. 290853), the European grant MC-RG ATTOTREND, the MICINN Project (No. FIS2010-15127), and the ERA-Chemistry Project (No. PIM2010EEC-00751).

[1] F. Krausz and M. Ivanov, Rev. Mod. Phys. **81**, 163 (2009).

[2] G. Sansone, F. Kelkensberg, J. F. Pérez-Torres, F. Morales, M. F. Kling, W. Siu, O. Ghafur, P. Johnsson, M. Swoboda, E. Benedetti, F. Ferrari, F. Lépine, J. L. Sanz-Vicario, S. Zherebtsov, I. Znakovskaya, A. L'Huillier, M. Yu. Ivanov, M. Nisoli, F. Martín, and M. J. J. Vrakking, Nature (London) **465**, 763 (2010).

[3] E. Goulielmakis, Z.H. Loh, A. Wirth, R. Santra, N. Rohringer, V. S. Yakovlev, S. Zherebtsov, T. Pfeifer, A. M. Azzeer, M. F. Kling, S. R. Leone, and F. Krausz, Nature (London) **466**, 739 (2010).

[4] M. Schultze, M. Fieß, N. Karpowicz, J. Gagnon, M. Korbman, M. Hofstetter, S. Neppl, A. L. Cavalieri, Y. Komninos, Th. Mercouris, C. A. Nicolaides, R. Pazourek, S. Nagele, J. Feist, J. Burgdörfer, A. M. Azzeer, R. Ernstorfer, R. Kienberger, U. Kleineberg, E. Goulielmakis, F. Krausz, and V. S. Yakovlev, Science **328**, 1658 (2010).

[5] H. Wang, M. Chini, S. Chen, C.-H. Zhang, F. He, Y. Cheng Y. Wu, U. Thumm, and Z. Chang, Phys. Rev. Lett. **105**, 143002 (2010).

[6] M. Holler, F. Schapper, L. Gallmann, and U. Keller, Phys. Rev. Lett. **106**, 123601 (2011).

[7] K. Klünder, J. M. Dahlström, M. Gisselbrecht, T. Fordell, M. Swoboda, D. Guénot, P. Johnsson, J. Caillat, J. Mauritsson, A. Maquet, R. Taïeb, and A. L'Huillier, Phys. Rev. Lett. **106**, 143002 (2011).

[8] H. Niikura, F. Légaré, R. Hasbani, A. D. Bandrauk, M. Y. Ivanov, D. M. Villeneuve, and P. B. Corkum, Nature (London) **417**, 917 (2002).

[9] J.-F. Hergott, M. Kovacev, H. Merdji, C. Hubert, Y. Mairesse, E. Jean, P. Breger, P. Agostini, B. Carré, and P. Salières, Phys. Rev. A **66**, 021801 (2002).

[10] P. Tzallas, D. Charalambidis, N. A. Papadogiannis, K. Witte, and G. D. Tsakiris, Nature (London) **426**, 267 (2003).

[11] Y. Nabekawa, T. Shimizu, T. Okino, K. Furusawa, H. Hasegawa, K. Yamanouchi, and K. Midorikawa, Phys. Rev. Lett. **96**, 083901 (2006).

[12] Y. Nomura, R. Hörlein, P. Tzallas, B. Dromey, S. Rykovanov, Zs. Major, J. Osterhoff, S. Karsch, L. Veisz, M. Zepf, D. Charalambidis, F. Krausz, and G. D. Tsakiris, Nat. Phys. **5**, 124 (2009).

[13] T. Popmintchev, M.-C. Chen, D. Popmintchev, P. Arpin, S. Brown, S. Ališauskas, G. Andriukaitis, T. Balčiunas, O. D. Mücke, A. Pugzlys, A. Baltuška, B. Shim, S. E. Schrauth, A. Gaeta, C. Hernández-García, L. Plaja, A. Becker, A. Jaron-Becker, M. M. Murnane, and H. C. Kapteyn, Science **336**, 1287 (2012).

[14] P. Tzallas, E. Skantzakis, C. Kalpouzos, E. P. Benis, G. D. Tsakiris, and D. Charalambidis, Nat. Phys. **3**, 846 (2007).

[15] H. Mashiko, S. Gilbertson, C. Li, S. D. Khan, M. M. Shakya, E. Moon, and Z. Chang, Phys. Rev. Lett. **100**, 103906 (2008).

[16] E. Skantzakis, P. Tzallas, J. Kruse, C. Kalpouzos, and D. Charalambidis, Opt. Lett. **34**, 1732 (2009).

[17] E. J. Takahashi, P. Lan, O. D. Mücke, Y. Nabekawa, and K. Midorikawa, Phys. Rev. Lett. **104**, 233901 (2010).

[18] F. Ferrari, F. Calegari, M. Lucchini, C. Vozzi, S. Stagira, G. Sansone, and M. Nisoli, Nature Photon. **4**, 875 (2010).

[19] E. J. Takahashi, P. Lan, O. D. Mücke, Y. Nabekawa, and K. Midorikawa (unpublished).

[20] E. Skantzakis, P. Tzallas, J. E. Kruse, C. Kalpouzos, O. Faucher, G. D. Tsakiris, and D. Charalambidis, Phys. Rev. Lett. **105**, 043902 (2010).

[21] P. Tzallas, E. Skantzakis, L. A. A. Nikolopoulos, G. D. Tsakiris, and D. Charalambidis, Nat. Phys. **7**, 781 (2011).

[22] P. Tzallas, E. Skantzakis, and D. Charalambidis, J. Phys. B **45**, 074007 (2012).

[23] A. González-Castrillo, A. Palacios, H. Bachau, and F. Martín, Phys. Rev. Lett. **108**, 063009 (2012).

[24] P. Tzallas, D. Charalambidis, N. A. Papadogiannis, K. Witte, and G. D. Tsakiris, J. Mod. Opt. **52**, 321 (2005).

[25] O. Faucher, P. Tzallas, E.P. Benis, J. Kruse, A. Peralta Conde, C. Kalpouzos, and D. Charalambidis, Appl. Phys. B **97**, 505 (2009).

[26] H. Mashiko, A. Suda, and K. Midorikawa, Appl. Phys. B **87**, 221 (2007).

[27] G. Kolliopoulos, B. Bergues, H. Schröder, P. A. Carpeggiani, L. Veisz, G. D. Tsakiris, D. Charalambidis, and P. Tzallas, arXiv:1307.3859.

[28] P. Tzallas, E. Skantzakis, and D. Charalambidis, Phys. Rev. A **82**, 061401(R) (2010).

[29] J. F. Pérez-Torres, J. L. Sanz-Vicario, H. Bachau, and F. Martín, J. Phys. B **43**, 015204 (2010).

[30] M. J. J. Vrakking, D. M. Villeneuve, and A. Stolow, Phys. Rev. A **54**, R37 (1996).